Published online 8 February 2007 *Nucleic Acids Research, 2007, Vol. 35, No. 5* ***1601–1611***
doi:10.1093/nar/gkm021

Rapid determination of the active fraction of DNA repair glycosylases: a novel fluorescence assay for trapped intermediates

Jeffrey O. Blaisdell and Susan S. Wallace*

Department of Microbiology and Molecular Genetics, Markey Center for Molecular Genetics, University of Vermont, Burlington, VT, USA

Received November 28, 2006; Revised December 22, 2006; Accepted January 2, 2007

ABSTRACT

Current methods to measure the fraction of active glycosylase molecules in a given enzyme preparation are slow and cumbersome. Here we report a novel assay for rapidly determining the active fraction based on molecular accessibility of a fluorescent DNA minor groove binder, 4′,6-diamidino-2-phenylindole (DAPI). Several 5,6-dihydrouracil-containing (DHU) DNA substrates were designed with sequence-dependent DAPI-binding sites to which base excision repair glycosylases were covalently trapped by reduction. Trapped complexes impeded the association of DAPI in a manner dependent on the enzyme used and the location of the DAPI-binding site in relation to the lesion. Of the sequences tested, one was shown to give an accurate measure of the fraction of active molecules for each enzyme tested from both the Fpg/Nei family and HhH-GPD Nth superfamily of DNA glycosylases. The validity of the approach was demonstrated by direct comparison with current gel-based methods. Additionally, the results are supported by *in silico* modeling based on available crystal structures.

INTRODUCTION

All nonobligate organisms possess repair systems responsible for the maintenance of genomic DNA in the presence of cellular reactive oxygen species (ROS). The majority of single base lesions generated by ROS are abstracted by DNA glycosylases as the initial step in the base excision repair pathway [for reviews, see (1,2)]. Mechanistically, these enzymes are classified by either the presence of an associated AP lyase activity (bifunctional), or the lack of this activity (monofunctional). Monofunctional glycosylases cleave the glycosyl bond via either an associative S_N2 reaction utilizing an activated water molecule or a dissociative S_N1-like mechanism. Bifunctional glycosylases employ an amine for nucleophilic (S_N2) attack of the sugar backbone, proceeding through a Schiff base intermediate which can undergo a β-elimination that leads to cleavage of the lesion-containing strand [for reviews, see (3,4)]. Enzymes whose mechanism proceed through a transient Schiff base intermediate can be trapped by the addition of a reducing agent such as $NaBH_4$ or $NaCNBH_3$ [for reviews, see (5)]. Once covalently bound, trapped molecules no longer participate in the overall reaction resulting in stable protein–DNA complexes.

The ability to efficiently generate stable, covalently bound glycosylase–DNA complexes has broad-reaching applications and has been used extensively in the literature. Studies utilizing this procedure include, but are not limited to, bifunctional versus monofunctional classification (6–8), determination of the fraction of active molecules in enzyme preparations (9,10), reaction rate analyses (11,12), glycosylase activity comparisons (13–15), iron–sulfur cluster domain analysis (16), and the characterization of enzyme active-site residues (10,17–21). A commonality among these techniques is the almost universal requirement for separation of the trapped complex from unbound DNA via polyacrylamide gel electrophoresis (PAGE) prior to phosphorimager analysis. It should be noted that while the characterization of active-site residues may alternatively employ tryptic digestion of the trapped complex in order to identify the bound peptide (20,21), targeted mutagenesis experiments require a gel-based approach (10,17–19). A gel-based approach may be necessary in some circumstances; for example, the determination of specific reaction intermediates (22). However, a faster, less cumbersome technique would be useful for the majority of situations.

The properties of 4′,6-diamidino-2-phenylindole (DAPI) have been well studied for more than 30 years, from pH and ionic strength influences (23,24) to the solved crystal structure of DAPI-DNA complexes (25,26).

*To whom correspondence should be addressed. Tel: +1 802 656 2164; Fax: +1 802 656 8749; Email: susan.wallace@uvm.edu

Similar to distamycin and its analogs, DAPI preferentially binds to the minor groove of AT-rich regions of double-stranded DNA (24,27–31). Due to its unique fluorescent characteristics (31) it has been employed successfully in various dye displacement assays (32,33). In this article, we describe a novel approach for using DAPI as a fluorescent reporter molecule to rapidly differentiate the number of bound versus unbound enzymes to damaged oligonucleotides following protein–DNA cross-linking. Although the focus of this work is on determining the fraction of active molecules in enzyme preparations, the technique is equally applicable to the studies listed above. Any study which necessitates analyzing the total number of trapped enzyme–DNA moieties, and does not require discrimination of the trapped intermediates themselves, may benefit from this approach. We foresee this molecular accessibility assay being useful in the study of numerous DNA-binding proteins.

MATERIALS AND METHODS

DNA substrates

Oligonucleotide substrates were purchased from Midland Certified Reagent Co. (Midland, TX) and were PAGE purified prior to use. All gel-based comparisons were performed with the following double-stranded substrate: (35DHU) 5′-TET-TGTCAATAGCAAGXGGAGAAGT CAATCGTGAGTCT-3′ where TET represents the fluorescent label 6-tetrachlorofluorescein and X = 5,6-dihydrouracil (DHU). Molecular accessibility DAPI-based experiments were performed with the following double-stranded substrates: (4L) 5′-GCCCCGCCAATTX CCGCCGCCGCC-3′, (5L) 5′-GCCCCGCCAATTCXCC GCCGCCGCC-3′, (5R) 5′-GCCCCGCCGCCCCGCCX AATTCCGCCGCCGCC-3′, and (N5R) 5′-GCCCCGCC GCCCCGCCXCAATTCCGCCGCCGCC-3′ where X = either DHU for damaged substrates or cytosine for non-damaged controls. All complementary strands contained a G residue across from DHU and were annealed in 50 mM Tris-HCl (pH 8.0), 50 mM NaCl by heating to 94°C for 2 min and slowly cooling to 4°C over the period of 1 h in a Perkin Elmer DNA Thermal Cycler 480. In each case the ratio of damaged to complementary strand during annealing was 1:1.1. Note that the DAPI-based oligonucleotides all differ in location of the AT-rich region in relation to the damaged base.

Purification of enzymes

Escherichia coli endonuclease III (EcoNth), formamidopyrimidine-DNA glycosylase (EcoFpg), endonuclease VIII (EcoNei), and its human ortholog (NEIL1) were purified by either the pET system (Novagen) or IMPACT CN system (New England Biolabs). A detailed protocol for cloning and expression of each of these recombinant proteins has been previously described (34).

Trapping of Schiff base intermediates

EcoNth, EcoFpg, EcoNei and NEIL1 were incubated for 30 min at 37°C with 100 nM DHU:G-containing substrates at final concentrations of 50, 100, 200, 400, 800, 1200 or 1600 nM, in the presence of either 50 or 100 mM sodium borohydride ($NaBH_4$) or sodium cyanoborohydride ($NaCNBH_3$), as described in the figures. Borohydride compounds were dissolved fresh for each independent experiment (one substrate and series of enzyme dilutions) as 1.25× stocks in Milli-Q water. Reactions were initiated by simultaneous addition of enzyme and borohydride solution to annealed substrates utilizing separate multi-pipettes in a 96-well format to a final volume of 100 µl. Except for EcoFpg trapping with sodium cyanoborohydride, the final buffer for each reaction contained 10 mM Tris-HCl (pH 8.0), 60 mM Na^+ and either 50 mM BH_4^- or $CNBH_3^-$. In the former case, the final buffer contained 10 mM Tris-HCl (pH 8.0), 110 mM Na^+ and 100 mM $CNBH_3^-$.

For gel-based substrates, completed reactions were mixed with a dye-free SDS loading buffer (50 mM Tris-HCl (pH 6.8), 100 mM dithiothreitol, 4% SDS, 10% glycerol), heated to 90°C for 5 min, separated by 12% SDS-PAGE, and visualized by phosphorimager analysis (Bio-Rad Molecular Imager FX). For all other substrates, an equal volume of 200 nM DAPI in 10 mM Tris-HCl (pH 8.0) and 50 mM NaCl was added and incubated for 5 min at room temperature prior to fluorescence detection. Final concentrations of the fluorescence effecting molecules at the time of detection in these experiments were 100 nM DAPI, 50 nM substrate, and 25–800 nM enzyme.

Fluorescence measurements

Fluorescence readings were made on a Synergy HT Multi-Detection Microplate Reader (BIO-TEK) using a tungsten-halogen lamp and 360/40 bandpass excitation filter in conjunction with a 460/40 emission filter. Corning Half Area, NBS treated (Nonbinding Surface), Black, 96-well Microplates (Corning #3686) were used for all DAPI-based experiments. The combination of enzymes, DNA and DAPI were all shown to contribute linearly to changes in the overall fluorescence based on the range of concentrations used; there was therefore no need to correct for the inner filter effect (data not shown).

Sodium cyanoborohydride optimization

Trapping and fluorescence detection were performed essentially as described above with 100 nM 4L substrate, 200 nM EcoFpg and final buffer concentrations of 10 mM Tris-HCl (pH 8.0), 60 mM Na^+, and 0–200 mM $CNBH_3^-$. The ionic strength contribution from sodium ions was held constant by varying the amount of the following compounds added to each reaction: sodium chloride, sodium cyanoborohydride, and/or tetrabutylammonium cyanoborohydride. Fluorescence was normalized to the first reading and plotted as a 36 segment cubic spline curve using Prism 4 (GraphPad Software).

Data analyses: determining the active fraction of molecules

Given a sufficiently high concentration of trapping reagent, and a sufficiently long incubation time, the quantity of ES complex is related to the quantity of

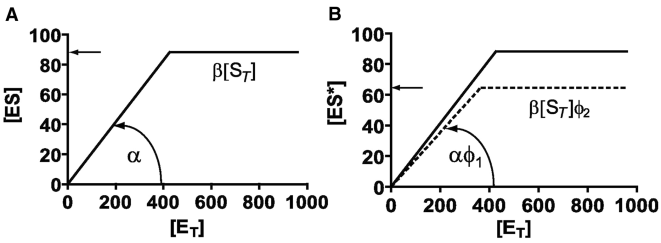

Figure 1. Theoretical plots for active fraction determination. (**A**) The quantity of ES complex formed in a standard gel-based Schiff base assay as related to the total enzyme concentration, E_T, plotted by the equation $ES = \min(\alpha E_T, \beta S_T)$, where α is the active enzyme fraction, β the fraction of cleavable substrate and S_T the total substrate added. (**B**) The dashed line represents the quantity of ES* complex formed in the DAPI molecular accessibility assay as related to the total enzyme concentration, E_T, plotted by the equation $ES = \min(\alpha E_T \Phi_1, \beta S_T \Phi_2)$, where α, β and S_T are as above, $0 \leq \Phi_{1,2} \leq 1$ is the accessibility parameter, and $ES^* \leq ES$.

total enzyme added, E_T, and total substrate added, S_T, by the equation: $ES = \min(\alpha E_T, \beta S_T)$ where α is the active enzyme fraction, β is the active substrate fraction (fraction cleavable), and min is the minimum function. Furthermore, holding S_T constant while varying E_T can be depicted graphically (Figure 1A) where the rising slope is equivalent to α, the plateau is equivalent to $S_T \times \beta$, and the breakpoint is defined by the relation: $S_T = (\alpha/\beta)E_T$. Therefore, by varying E_T from below to well above the constant S_T concentration, the active enzyme fraction can be determined by linear regression of all points falling below the E_T breakpoint concentration. The decision to include or exclude a given point as pre-breakpoint is simply made so as to minimize the root-mean squared deviation from both the pre-breakpoint regression and the post-breakpoint best-fit line with a slope of zero.

For gel-based assays, the active enzyme fraction was determined following PhosphorImager analysis from the relative amounts of trapped to non-trapped DNA by the α-value method described above. For the molecular accessibility assays, the active fraction was determined from relative fluorescence values also using the α-value method (note that an increase in trapped enzyme complex translates to a decrease in detected fluorescence). We hypothesized that the location of the DAPI-binding site in relation to the trapped enzyme would affect the total detected fluorescence, possibly leading to a lower quantity of ES complex detected on some sequences. This is depicted in Figure 1B such that the determination of trapped complex can be described as: $ES^* = \min(\alpha E_T \Phi_1, \beta S_T \Phi_2)$ where $0 \leq \Phi_{1,2} \leq 1$ is an accessibility parameter and $ES^* \leq ES$. Complete association of DAPI, independent of the quantity of trapped ES complex, would have an accessibility parameter equal to 0. In contrast, association which is perfectly dependent on the quantity of trapped ES complex would have accessibility parameter of 1, and therefore ES* equals ES. In this study, we show the existence of an oligonucleotide sequence (4L) where Φ approaches 1 for several DNA glycosylases from different phylogenetic families.

Molecular modeling

Modeling for the illustrations shown in Figure 2, and for the results listed in Table 1 was performed using the PyMol Molecular Graphics System (DeLano,W.L., 2002, http://www.pymol.org) as follows: two published structures of DAPI–DNA complexes, AATT localized from 1D30.pdb (25) and the proposed ATTG shifted localization from 432D.pdb (26,35), were molecularly superimposed onto the published BstNth and EcoFpg Schiff base intermediate-trapped structures 1ORN.pdb (36) and 1K82.pdb (37), respectively. Alignment was made using the phosphate backbone of the AATT region of the DAPI structures and the corresponding phosphate backbone of each enzyme–DNA structure for both possible orientations of DAPI (due to non-symmetry of the dye and target). The pair_fit command was used to minimize the root mean square deviation (RMSD) of each atom in the alignment. In total, the 32-modeled structures were fit by alignment of 66, 85 or 88 atoms with RMSD values of the fit ranging from 0.765 to 1.815 Å.

RESULTS

Fluorescence of DAPI-bound DNA substrates

Each of the 4L, 5L, 5R and N5R substrates, along with their non-damaged counterparts, were initially tested for their ability to associate with DAPI and thereby affect the detected fluorescence. As can be seen in Table 2, each of the sequences showed a significant increase in fluorescence over background. In the absence of DNA, there was only a small increase in fluorescence from the addition of DAPI, as would be expected. The differences in fluorescence for each of the DAPI-bound substrates are presumably due to both sequence context and experimental variations in DNA concentration. For example, the 4L sequence is expected to have a lower total fluorescence due to the importance of the 3′ nucleotide following the 5′-AATT-3′ binding sequence in regards to fluorescence intensity (38). Due to the fact that the molecular accessibility assay is based on relative fluorescence, these differences are inconsequential. Non-damaged substrates, where the DHU base is replaced with cytosine, were also tested; the fluorescence levels of these substrates were statistically equal to their damaged counterparts with the exception of the 4L(−) context, which showed an expected increase from the introduction of cytosine in the 5′-AATTC-3′ sequence.

EcoNth: DAPI accessibility emulates gel-based results

In order to validate the results of the molecular accessibility assay, we first determined the active fraction of a preparation of EcoNth via traditional gel-based methods. As shown in Figure 3A and C, the α values were determined to be 0.199 and 0.206 for experiments using $NaBH_4$ and $NaCNBH_3$ as reducing agents, respectively. This corresponds to an active fraction of ~20%. The β value, though of little importance in the context of this article, was determined to be ~0.8, which is consistent with the active fraction of substrates used in

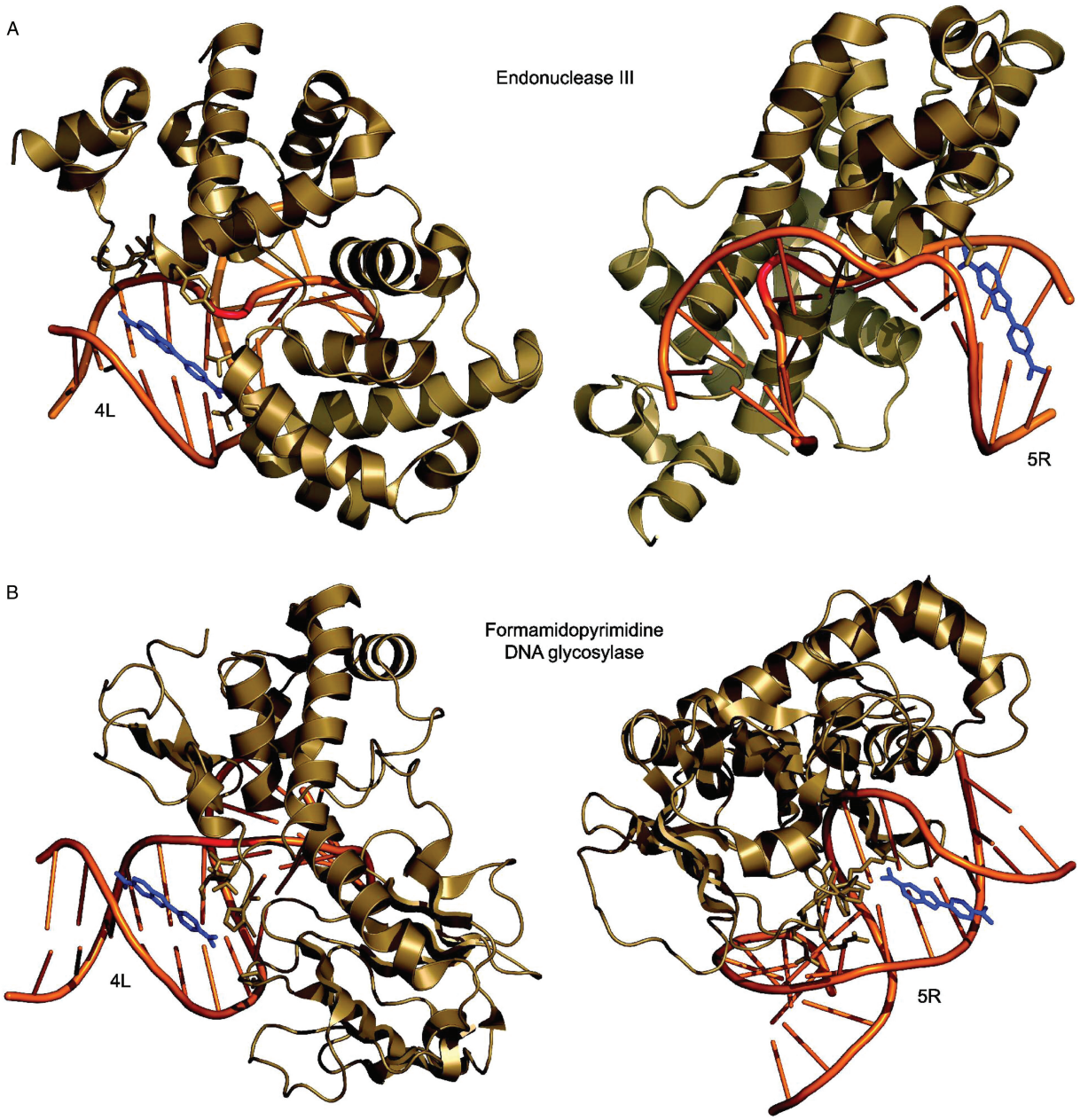

Figure 2. Molecular modeling of BstNth and EcoFpg with DAPI. One orientation of DAPI is shown in the predicted binding location with BstNth and the 4L substrate (**A**, left) or the 5R substrate (**A**, right). The same orientations of DAPI are also shown with EcoFpg and the 4L substrate (**B**, left) or the 5R substrate (**B**, right). Note the orientation of the minor groove at the DAPI-binding site in each case. See the materials and methods section for details describing the creation of these models. See Table 1 for a summary of predicted binding locations with each enzyme and substrate combination.

our laboratory. For each data plot, the α and β values were calculated as depicted in Figure 1, and as described in the materials and methods section. The total amount of trapped complex was determined from the sum of each shifted band in a given lane. The occurrence of multiple gel-shifted bands is a consequence of the trapping of intermediates along the reaction pathway and their separation via SDS-PAGE (22). It should be noted that the molecular accessibility assay will not distinguish between reaction intermediates; a single fluorescent reading for each enzyme concentration point is generated for all trapped complexes. For this reason, considering the difficulties associated with accurately measuring pixel intensities, the DAPI-based approach is more accurate.

Results of the molecular accessibility assay for each of the sequence contexts and reducing agents used are shown in Figure 3B and D. The calculated α values for the 4L, 5L and 5R sequences ranged from 0.188 to 0.243 giving an active fraction range of ~19–24%, consistent with the gel-based results. The calculated α values for the N5R sequence were lower, giving associated active fractions of ~12% and 16%, presumably due to the ability

Table 1. Molecular modeling summary of DAPI bound to trapped enzyme–DNA complexes. The distance in angstroms is shown for the two closest atoms between DAPI and either BstNth or EcoFpg. Both of the known DAPI-binding modes based on crystal structure data, AATT and ATTG, for each of the two possible DAPI orientations (separated by commas) are listed. The last column specifies the orientation of the minor groove where DAPI binds, in relation to the trapped protein. See the materials and methods section for details describing the creation of these modeling summaries.

Complex	AATT	ATTG	Minor groove
Nth-4L	1.54, 1.70[b]	1.85, 1.50[b]	Internal face
Nth-5L	2.36, 2.55	1.56, 2.09	Internal face
Nth-5R	2.13[b], 2.32	2.21[b], 3.10	External face
Nth-N5R	2.51, 4.41	2.96, 7.87	External face
Fpg-4L	4.97, 4.51[b]	6.26, 1.58[b]	Internal face
Fpg-5L	5.01, 7.33	4.09, 10.8[a]	Internal face
Fpg-5R	0.72[b], 1.33	1.19[b], 3.23	External face
Fpg-N5R	2.54, 4.67	1.51, 7.16	External face

[a]externally facing exception due to distance from protein.
[b]orientation unlikely to occur due to the disruption of one or more hydrogen bonds with the cleaved DNA base.

Table 2. Fluorescence of DAPI binding to double-stranded DNA. Each double-stranded DNA, at a concentration of 50 nM, was incubated with 100 nM DAPI in 10 mM Tris-HCl (pH 8.0) and 50 mM NaCl for 5 min at room temperature and fluorescence was detected on a Synergy HT Multi-Detection Microplate Reader. X = DHU. All complementary strands contained a G residue across from DHU. See the materials and methods section for the complete oligonucleotide sequences.

dsDNA	Subsequence	DAPI	F_I[a]
4L	5′-CCAATTXC-3′	+	55.2 ± 2.8
4L(−)	5′-CCAATTCC-3′	+	62.4 ± 2.3
5L	5′-CCAATTCX-3′	+	65.9 ± 2.6
5L(−)	5′-CCAATTCC-3′	+	63.3 ± 4.3
5R	5′-CXAATTCC-3′	+	69.5 ± 2.9
5R(−)	5′-CCAATTCC-3′	+	63.7 ± 3.4
N5R	5′-XCAATTCC-3′	+	60.7 ± 3.0
N5R(−)	5′-CCAATTCC-3′	+	60.7 ± 3.1
–	n/a	+	5.0 ± 0.4
–	n/a	–	2.7 ± 0.1

[a]F_I = Fluorescence intensity $\times 10^{-3}$.

of DAPI to associate with the EcoNth–N5R trapped complex. Interestingly, both the 5R and N5R sequences showed lower then expected β values, suggesting at least some association of DAPI with the EcoNth–5R trapped complex as well.

In order to further elucidate the above results, DAPI was modeled into its predicted binding locations for each complex using a *Bacillus stearothermophilus* endonuclease III trapped intermediate, as described in the materials and methods section. Association of DAPI with a trapped complex is modulated by two main factors, steric hindrance between any 'close contacts' and orientation of the minor groove at the DAPI-binding site in relation to the protein. Figure 2A shows two predicted binding locations: one orientation of DAPI bound to the 5′-AATT-3′ site with BstNth-4L (left) and one with BstNth-5R (right). In the 4L sequence the minor groove where DAPI binds is on an internal face, protected by the enzyme. With the 5R sequence however, the minor groove is exposed such that DAPI association can only be inhibited by steric hindrance from close amino acids. The top half of Table 1 summarizes the BstNth modeling results with regard to close contacts and minor groove location, for each predicted binding mode and orientation. As can be seen, steric hindrance predicts that the 4L, 5L and possibly 5R sequences should accurately determine the active fraction. Additionally, both the 4L and 5L sequences benefit from having the minor groove where DAPI binds in a protected location. These modeling data support the results shown in Figure 3B and D, providing further evidence of the validity of this assay.

EcoFpg: DAPI accessibility emulates gel-based results

Similar to above, we also determined the active fraction of a preparation of EcoFpg via traditional gel-based methods. As shown in Figure 4A and C, the α values were determined to be 0.121 and 0.147 depending on the reducing agent used—corresponding to an active fraction of ∼13%. The β value was again ∼0.8. Notably, when using 100 mM sodium cyanoborohydride as a reducing agent (Figure 4C), a small amount of product was generated. The quantity of product is small enough so that its inclusion or exclusion during analysis only affects the determined α value by ∼1.5% (data not shown). However, the importance of limiting product generation is paramount and is discussed in detail below. Results of the molecular accessibility assay for each of the sequence contexts and reducing agents used with EcoFpg are shown in Figure 4B and D. The calculated α values for the 4L sequence were 0.154 and 0.136 giving an active fraction of ∼14%, consistent with the gel-based results. The calculated α values for the 5R sequence were slightly lower giving an ∼11% active fraction, and both the 5L and N5R sequences were significantly lower. The apparent β values were significantly lower for the 5L, 5R and N5R sequences, suggesting increased association of DAPI with the EcoFpg–DNA trapped complex, and therefore a smaller accessibility parameter, Φ. The apparent β value for the 4L sequence was ∼0.7 in these experiments. Re-testing with EcoNth verified that the 10% drop in β value for the 4L substrate was accurate (data not shown), and was presumably caused from prolonged storage of the annealed, DHU-containing substrate at 4°C.

As was done with BstNth, modeling of DAPI into the predicted binding locations for each of the trapped EcoFpg–DNA complexes was performed as described in the materials and methods section and is illustrated for two cases in Figure 2B. Once again, the 4L sequence protects the minor groove of the drug-binding site, while the 5R sequence exposes the 5′-AATT-3′ minor groove. The bottom half of Table 1 summarizes the EcoFpg modeling results for all predicted binding sites, for each DNA sequence. Interestingly, only the enzyme-trapped 5R sequence predicts any steric hindrance with regard to DAPI binding. For each of the other sequences there is at least one orientation of DAPI with significant steric freedom. This includes the 4L sequence, which was already shown to accurately determine the active fraction of enzyme in Figure 4. This result highlights the

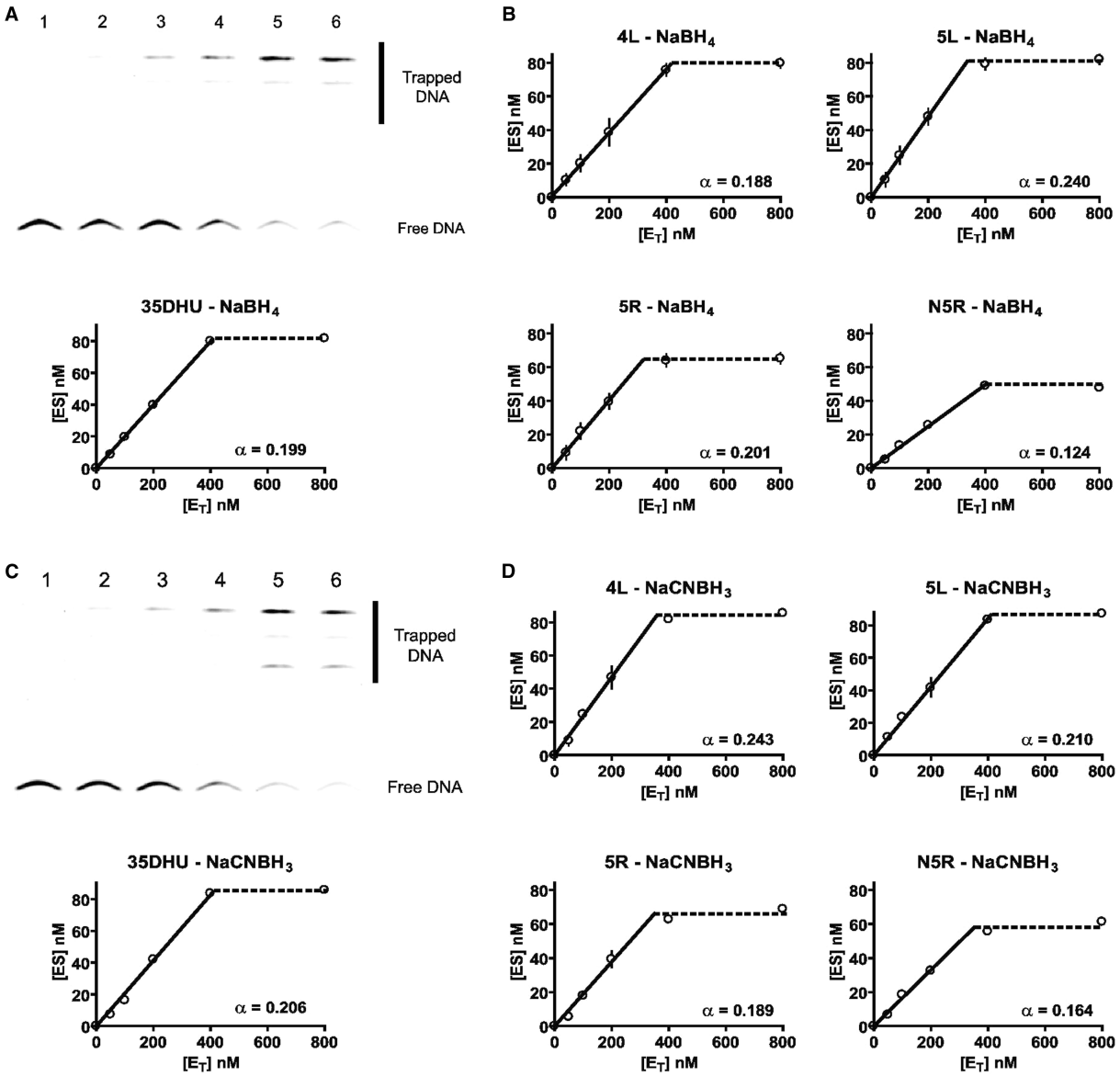

Figure 3. EcoNth active fraction determination by gel-based and molecular accessibility assays. 0, 50, 100, 200, 400 and 800 nM EcoNth was incubated for 30 min at 37°C with either 100 nM of 35DHU substrate (**A** and **C**) or 100 nM of 4L, 5L, 5R or N5R substrates (**B** and **D**) in the presence of either 50 mM sodium borohydride (**A** + **B**) or 50 mM sodium cyanoborohydride (**C** + **D**). Completed 35DHU reactions were separated by 12% SDS-PAGE; results from phosphorimager analysis with calculated α values are plotted below each gel image. Completed 4L, 5L, 5R and N5R reactions were mixed with an equal volume of 200 nM DAPI solution, incubated for 5 min at room temperature, and fluorescence was detected at 340 nm excitation/460 nm emission. Relative fluorescence readings to the 0 nM EcoNth sample were used to determine the concentration of ES complex at each enzyme concentration. Error bars representing the standard deviation from three independent experiments are shown on all points where the error was larger than the body of the symbol. See the materials and methods section for further details of experimental design and analysis.

importance of the orientation of the minor groove at the DAPI-binding site, and predicts the practicality of using the 4L substrate for numerous DNA glycosylases regardless of active site binding differences. Noting the importance of the minor groove orientation, the modeling data again support the molecular accessibility assay results.

Optimizing the concentration of reducing agent

Optimizing the concentration of reducing agent used is an important step for any trapping assay. It is, however, of particular importance for accurately determining the active fraction by DAPI association. Fully cleaved 4L substrate shows approximately one-half the maximal fluorescence compared to uncleaved substrate, due to a higher rate of DAPI dissociation (data not shown). The increased dissociation rate of the dye is presumably caused by the single-strand nick 3′ of the binding site. Nevertheless, the effect of this characteristic would be an increase in apparent trapped complex in situations where significantly high quantities of product are allowed to form, leading to an artificially high α value and lower β value. To avoid this, the accessibility assay itself can be

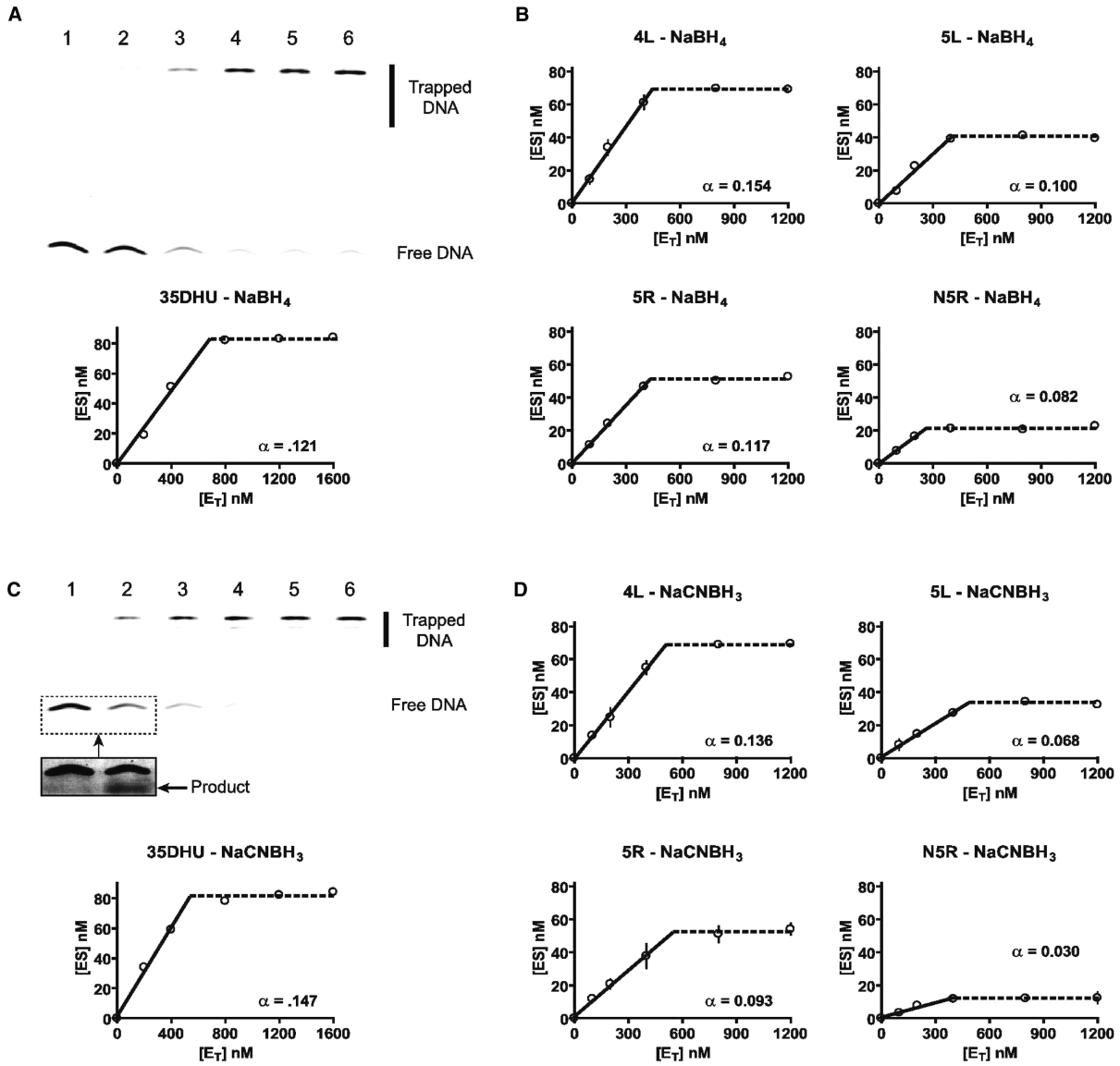

Figure 4. EcoFpg active fraction determination by gel-based and molecular accessibility assays. 0, 200, 400, 800, 1200 and 1600 nM EcoFpg was incubated for 30 min at 37°C with either 100 nM of 35DHU substrate (**A** and **C**) or 100 nM of 4L, 5L, 5R or N5R substrates (**B** and **D**) in the presence of either 50 mM sodium borohydride (**A** + **B**) or 100 mM sodium cyanoborohydride (**C** + **D**). Completed 35DHU reactions were separated by 12% SDS-PAGE; results from PhosphorImager analysis with calculated α values are plotted below each gel image. Completed 4L, 5L, 5R and N5R reactions were mixed with an equal volume of 200 nM DAPI solution, incubated for 5 min at room temperature, and fluorescence was detected at 340 nm excitation/460 nm emission. Relative fluorescence readings to the 0 nM EcoFpg sample were used to determine the concentration of ES complex at each enzyme concentration. Error bars representing the standard deviation from three independent experiments are shown on all points where the error was larger than the body of the symbol. See the materials and methods section for further details of experimental design and analysis.

used to quickly optimize the concentration of reducing agent. Figure 5 shows a typical optimization experiment where sodium cyanoborohydride concentration is optimized for one concentration of EcoFpg. As the concentration of reducing agent initially increases we see a substantial drop in the apparent concentration of trapped complex. This drop is expected based on the fact that a higher percentage of active enzyme molecules are being trapped before they are able to turnover a significant amount of product. Beyond 50 mM $NaCNBH_3$ we see that there is an inflection point in the graph where increases in reducing agent concentration more efficiently lead to trapped complexes while limiting the production of product. The final inflection point at ~100 mM $NaCNBH_3$ is the optimal concentration for this reducing agent with this specific enzyme; higher concentrations prove inhibitory. The magnitude of each inflection point is specific to the enzyme used and to the active fraction of the enzyme in the preparation being tested. Finally, one should note the importance of maintaining ionic strength even at higher reducing agent concentrations, by using compounds such as tetrabutylammonium cyanoborohydride.

As shown in Figure 5, the optimal cyanoborohydride concentration was determined to be 100 mM. This concentration was used for the experiments shown in Figure 4C,

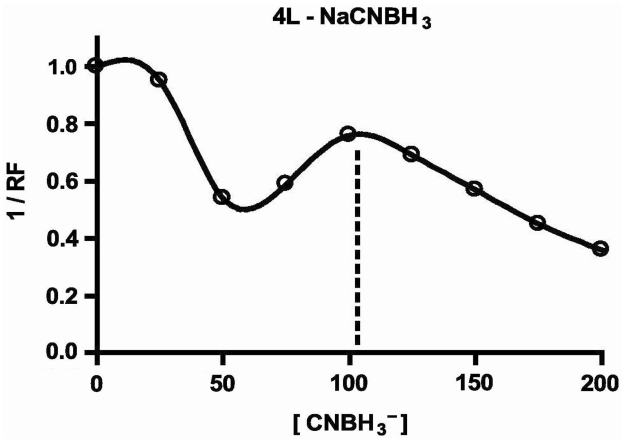

Figure 5. Reducing agent optimization with the molecular accessibility assay. EcoFpg, at a concentration of 200 nM, was incubated for 30 min at 37°C with 100 nM 4L substrate in the presence of 0–200 mM cyanoborohydride ion. Tetrabutylammonium cyanoborohydride was used at high concentrations to maintain similar ionic strengths in each reaction. Fluorescence was normalized to the first reading and plotted as inverse relative fluorescence versus $CNBH_3^-$ concentration on a cubic spline curve. See the materials and methods section for further details.

	Relative Fluorescence	
$[E_T]$	NEIL1	EcoNei
0	1.0	1.0
50	0.74	nd
100	0.49	0.98
200	nd	0.90
α	0.504	0.044
Activity	50.4 %	4.4 %

$[ES] = S_T * (1 - RF)$

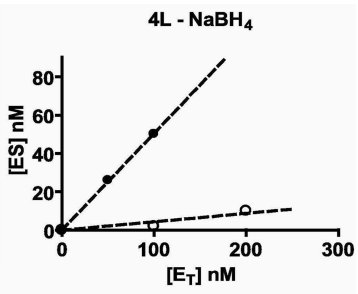

Figure 6. NEIL1 and EcoNei active fraction determination by the molecular accessibility assay. NEIL1, at concentrations of 50 and 100 nM, and EcoNei, at concentrations of 100 and 200 nM, were incubated with 100 nM 4L substrate in the presence of 50 mM sodium borohydride. Completed reactions were mixed with an equal volume of 200 nM DAPI solution, incubated for 5 min at room temperature, and fluorescence was detected at 340 nm excitation/460 nm emission. Relative fluorescence readings to the 0 nM enzyme sample were used to determine the concentration of ES complex using the equation $ES = S_T \times (1 - RF)$ where RF is the relative fluorescence at each given enzyme concentration, as shown in the table (left). Plotted ES concentrations (right) were used to determine the α values by linear regression. Activity is simply defined as the percentage of determined α values ($100 \times \alpha$). NEIL1, solid circles; EcoNei, open circles.

yet a small amount of product was still detected. Therefore, the use of a stronger reducing agent like $NaBH_4$ is recommended. While one could use $NaBH_4$ exclusively, the concurrent use of $NaCNBH_3$ provides a beneficial level of redundancy and comparisons between the two provide good evidence concerning the generation of a significant quantity of product.

DAPI accessibility with different enzyme preparations

To demonstrate the use of the accessibility assay with enzyme preparations having significantly different activities, two additional preparations were analyzed with the 4L substrate: an EcoNei purification known to have little activity and a more recent NEIL1 purification with good activity. Two concentrations were chosen for each, reflecting the prior knowledge of activity levels, and the desire to determine only the α values with a minimal amount of enzyme. Figure 6 shows results from the assay, and gives further detail into the calculation of ES concentration based on relative fluorescence. The accessibility assay was able to accurately determine the α value for both the EcoNei preparation, with less than 5% activity, and the NEIL1 preparation, with over 50% activity. Each of these was verified to be correct by traditional gel-based methods (data not shown).

DISCUSSION

In this article, we have described a novel approach to rapidly differentiate the number of bound versus unbound enzymes to damaged oligonucleotides following Schiff base trapping. Though the assay described focused on determining the fraction of active molecules in enzyme preparations, the technique itself should be applicable to any study which necessitates quantifying the total number of bound enzyme–DNA moieties. Previous approaches have been limited to either a traditional PAGE analysis or to the analysis of specific enzymes; for example, activity determination via the burst phase for glycosylases with slow product release (39).

For either the gel-based or DAPI-based approach, the crucial step is the ability to form trapped enzyme–DNA complexes. Though Schiff base formation is typically limited to bifunctional glycosylases, some monofunctional glycosylases may also be trapped by borohydride reduction (40,41). For monofunctional glycosylases which cannot be trapped via borohydride reduction, alternative trapping agents might prove useful. The use of 2-deoxyribonolactone and oxanine are both promising covalent trapping agents for various bifunctional and monofunctional glycosylases (42–45). The use of these compounds for active fraction analysis is currently being investigated.

Throughout this study a single damaged nucleotide, DHU, was used for all substrates. While this is adequate for comparisons made as a proof of concept, accurate determination of the active fraction of numerous enzymes requires additional substrates. For example, for accurate determination of the active fraction of EcoFpg, 7,8-dihydro-8-oxoguanine (8-oxoG) should be used based on the greater affinity for that damage. Some damaged nucleotides, such as 5-formyluracil, would be inappropriate for the activity determination of certain enzymes, due to their low affinity for the damage (13). The 'best' substrate for a given enzyme, based on prior knowledge, should always be used for accurate activity calculations. For previously uncharacterized enzymes, analysis of numerous substrates is required. Strong reducing agents, such as $NaBH_4$, should not be used in combination with damages which are extremely prone to reduction such as AP sites. In these cases, the use of $NaCNBH_3$, where the

half-life of an AP site has been reported to be about 6 h, is required (22). Regardless, it should also be noted that partial destruction of the substrate via reduction will not affect calculation of the α value, only the β value will be affected. With either the gel-based or DAPI-based methods, a strong reducing environment may possibly lead to inactivation of some enzyme molecules. Nonetheless, it is unlikely that both $NaBH_4$ and $NaCNBH_3$ will show the same rate of inactivation due to the inherent differences in their rate of reduction. A side-by-side test with both reducing agents (as was done in Figures 3 and 4) is arguably a valid control for demonstrating the lack of enzyme inactivation.

The accessibility, and inaccessibility, of the reporter dye to its binding site is obviously a hallmark of this assay. The preference of DNA minor groove-binding drugs for AT-rich sequences is thought to be primarily due to the narrow minor groove width which influences hydrogen bonding and van der Waals' interactions, and interrelationships of the positively charged amino ends of the drugs with the more negatively charged minor groove of AT sequences (46–50). The choice to use DAPI was primarily based on its well-known binding properties, ease of use with our current fluorimeter and the success of its use in other fluorescence assays (32,33). That said, other minor groove-binding dyes may prove useful in accessibility assays, notably ones with a larger minor groove footprint.

Comparing results of the molecular accessibility assay with the modeling results presented in Table 1, a number of insights can be drawn. Notably, when either EcoNth or EcoFpg was trapped with the 5R substrate, a lower accessibility parameter, Φ, was apparent. In each case, particularly with EcoFpg, the only predicted binding mode of DAPI with a greater than 3 Å distance from the enzyme is the ATTG-binding mode. When this structure was published, the authors were unable to unequivocally state that this AT/GC binding mode was sequence specific and not simply an artifact of crystal packing (26). The data presented here provide further evidence of alternative DAPI-binding modes, and does not rule out the possibility of the AT/GC association. No claims can be made, however, on the preference of one binding site over another.

As mentioned above, drug association may be modulated by either steric hindrance from the enzyme at the predicted DAPI-binding site and/or protection of the DAPI-binding site by orientation of the minor groove in relation to the protein. The fact that EcoFpg and the 4L substrate can accurately determine the active enzyme fraction (Figure 4B and D), and that both predicted binding modes for the EcoFpg–4L trapped complex have at least one orientation of DAPI which is not sterically hindered (Table 1), suggests that orientation of the DAPI-binding site is the more important contributor in modulating association. It should be noted that although the 5L substrate is generally classified as 'internally facing', one orientation of DAPI in the ATTG binding mode with trapped EcoFpg is externally facing due to the distance of DAPI from the enzyme. It is presumably for this reason that the 5L substrate is unable to accurately determine the active fraction with EcoFpg, since the other predicted binding configurations have internally facing DAPI-binding sites.

In this study, we have demonstrated a rapid, fluorescence-based approach for determining the number of bound versus unbound BER enzymes to damaged oligonucleotides following Schiff base trapping. The use of the 4L sequence context correctly determines enzyme activity from relative fluorescence calculations (no calibration necessary), for numerous DNA glycosylases from multiple phylogenetic families. The total experimental time is reduced from the standard 1–2 days using a traditional gel-based method, to under 1 h for the DAPI-based method. In a 96-well microplate format, the number of concurrent samples which can be tested also scales well. Additionally, neither radioactive nor fluorescent labels are required for substrate DNA. These benefits have allowed us to undertake frequent activity monitoring of enzyme stocks in our laboratory. One enzyme in particular has been found to drop from over 80% activity to 20% within a matter of weeks after initial purification. The testing of numerous optimized storage conditions can now be accomplished in minimal time. In conclusion, the molecular accessibility assay, specifically in conjunction with DAPI and the 4L substrate, should be useful in the study of numerous DNA-binding proteins.

ACKNOWLEDGEMENTS

The authors would like to thank Alicia Holmes for purification of the enzymes used in this study. PhosphorImager analysis was performed in the Vermont Cancer Center DNA Analysis facility. This research was funded by National Institutes of Health Public Health Service Grant P01CA098993 awarded by the National Cancer Institute. Funding to pay the Open Access publication charge was provided by National Institutes of Health.

Conflict of interest statement: None declared.

REFERENCES

1. Huffman,J.L., Sundheim,O. and Tainer,J.A. (2005) DNA base damage recognition and removal: new twists and grooves. *Mutat. Res.*, **577**, 55–76.
2. Wallace,S.S. (2002) Biological consequences of free radical-damaged DNA bases. *Free Radic. Biol. Med.*, **33**, 1–14.
3. Berti,P.J. and McCann,J.A. (2006) Toward a detailed understanding of base excision repair enzymes: transition state and mechanistic analyses of N-glycoside hydrolysis and N-glycoside transfer. *Chem. Rev.*, **106**, 506–555.
4. Stivers,J.T. and Jiang,Y.L. (2003) A mechanistic perspective on the chemistry of DNA repair glycosylases. *Chem. Rev.*, **103**, 2729–2759.
5. Verdine,G.L. and Norman,D.P. (2003) Covalent trapping of protein-DNA complexes. *Annu. Rev. Biochem.*, **72**, 337–366.
6. Im,E.K., Hong,C.H., Back,J.H., Han,Y.S. and Chung,J.H. (2005) Functional identification of an 8-oxoguanine specific endonuclease from Thermotoga maritima. *J. Biochem. Mol. Biol.*, **38**, 676–682.
7. Bandaru,V., Sunkara,S., Wallace,S.S. and Bond,J.P. (2002) A novel human DNA glycosylase that removes oxidative DNA damage and is homologous to Escherichia coli endonuclease VIII. *DNA Repair (Amst.)*, **1**, 517–529.

8. Dany,A.L. and Tissier,A. (2001) A functional OGG1 homologue from Arabidopsis thaliana. *Mol. Genet. Genomics*, **265**, 293–301.
9. Ikeda,S., Biswas,T., Roy,R., Izumi,T., Boldogh,I., Kurosky,A., Sarker,A.H., Seki,S. and Mitra,S. (1998) Purification and characterization of human NTH1, a homolog of Escherichia coli endonuclease III. Direct identification of Lys-212 as the active nucleophilic residue. *J. Biol. Chem.*, **273**, 21585–21593.
10. Burgess,S., Jaruga,P., Dodson,M.L., Dizdaroglu,M. and Lloyd,R.S. (2002) Determination of active site residues in Escherichia coli endonuclease VIII. *J. Biol. Chem.*, **277**, 2938–2944.
11. Zharkov,D.O., Rosenquist,T.A., Gerchman,S.E. and Grollman,A.P. (2000) Substrate specificity and reaction mechanism of murine 8-oxoguanine-DNA glycosylase. *J. Biol. Chem.*, **275**, 28607–28617.
12. Marenstein,D.R., Ocampo,M.T., Chan,M.K., Altamirano,A., Basu,A.K., Boorstein,R.J., Cunningham,R.P. and Teebor,G.W. (2001) Stimulation of human endonuclease III by Y box-binding protein 1 (DNA-binding protein B). Interaction between a base excision repair enzyme and a transcription factor. *J. Biol. Chem.*, **276**, 21242–21249.
13. Matsubara,M., Masaoka,A., Tanaka,T., Miyano,T., Kato,N., Terato,H., Ohyama,Y., Iwai,S. and Ide,H. (2003) Mammalian 5-formyluracil-DNA glycosylase. 1. Identification and characterization of a novel activity that releases 5-formyluracil from DNA. *Biochemistry*, **42**, 4993–5002.
14. Doi,Y., Katafuchi,A., Fujiwara,Y., Hitomi,K., Tainer,J.A., Ide,H. and Iwai,S. (2006) Synthesis and characterization of oligonucleotides containing 2′-fluorinated thymidine glycol as inhibitors of the endonuclease III reaction. *Nucleic Acids Res.*, **34**, 1540–1551.
15. Back,J.H., Park,J.H., Chung,J.H., Kim,D.S. and Han,Y.S. (2006) A distinct TthMutY bifunctional glycosylase that hydrolyzes not only adenine but also thymine opposite 8-oxoguanine in the hyperthermophilic bacterium, Thermus thermophilus. *DNA Repair (Amst.)*, **5**, 894–903.
16. Lu,A.L. and Wright,P.M. (2003) Characterization of an Escherichia coli mutant MutY with a cysteine to alanine mutation at the iron-sulfur cluster domain. *Biochemistry*, **42**, 3742–3750.
17. Sidorkina,O.M. and Laval,J. (2000) Role of the N-terminal proline residue in the catalytic activities of the Escherichia coli Fpg protein. *J. Biol. Chem.*, **275**, 9924–9929.
18. Saparbaev,M., Sidorkina,O.M., Jurado,J., Privezentzev,C.V., Greenberg,M.M. and Laval,J. (2002) Repair of oxidized purines and damaged pyrimidines by E. coli Fpg protein: different roles of proline 2 and lysine 57 residues. *Environ. Mol. Mutagen.*, **39**, 10–17.
19. Zharkov,D.O., Gilboa,R., Yagil,I., Kycia,J.H., Gerchman,S.E., Shoham,G. and Grollman,A.P. (2000) Role for lysine 142 in the excision of adenine from A:G mispairs by MutY DNA glycosylase of Escherichia coli. *Biochemistry*, **39**, 14768–14778.
20. Rieger,R.A., McTigue,M.M., Kycia,J.H., Gerchman,S.E., Grollman,A.P. and Iden,C.R. (2000) Characterization of a cross-linked DNA-endonuclease VIII repair complex by electrospray ionization mass spectrometry. *J. Am. Soc. Mass Spectrom.*, **11**, 505–515.
21. Zharkov,D.O., Rieger,R.A., Iden,C.R. and Grollman,A.P. (1997) NH2-terminal proline acts as a nucleophile in the glycosylase/AP-lyase reaction catalyzed by Escherichia coli formamidopyrimidine-DNA glycosylase (Fpg) protein. *J. Biol. Chem.*, **272**, 5335–5341.
22. Manuel,R.C., Hitomi,K., Arvai,A.S., House,P.G., Kurtz,A.J., Dodson,M.L., McCullough,A.K., Tainer,J.A. and Lloyd,R.S. (2004) Reaction intermediates in the catalytic mechanism of Escherichia coli MutY DNA glycosylase. *J. Biol. Chem.*, **279**, 46930–46939.
23. Kapuscinski,J. and Skoczylas,B. (1978) Fluorescent complexes of DNA with DAPI 4′,6-diamidine-2-phenyl indole.2HCl or DCI 4′,6-dicarboxyamide-2-phenyl indole. *Nucleic Acids Res.*, **5**, 3775–3799.
24. Manzini,G., Barcellona,M.L., Avitabile,M. and Quadrifoglio,F. (1983) Interaction of diamidino-2-phenylindole (DAPI) with natural and synthetic nucleic acids. *Nucleic Acids Res.*, **11**, 8861–8876.
25. Larsen,T.A., Goodsell,D.S., Cascio,D., Grzeskowiak,K. and Dickerson,R.E. (1989) The structure of DAPI bound to DNA. *J. Biomol. Struct. Dyn.*, **7**, 477–491.
26. Vlieghe,D., Sponer,J. and Van Meervelt,L. (1999) Crystal structure of d(GGCCAATTGG) complexed with DAPI reveals novel binding mode. *Biochemistry*, **38**, 16443–16451.
27. Trotta,E., D'Ambrosio,E., Del Grosso,N., Ravagnan,G., Cirilli,M. and Paci,M. (1993) 1H NMR study of [d(GCGATCGC)]2 and its interaction with minor groove binding 4',6-diamidino-2-phenylindole. *J. Biol. Chem.*, **268**, 3944–3951.
28. Wilson,W.D., Tanious,F.A., Barton,H.J., Jones,R.L., Fox,K., Wydra,R.L. and Strekowski,L. (1990) DNA sequence dependent binding modes of 4′,6-diamidino-2-phenylindole (DAPI). *Biochemistry*, **29**, 8452–8461.
29. Mohan,S. and Yathindra,N. (1994) A study of the interaction of DAPI with DNA containing AT and non-AT sequences—molecular specificity of minor groove binding drugs. *J. Biomol. Struct. Dyn.*, **11**, 849–867.
30. Albert,F.G., Eckdahl,T.T., Fitzgerald,D.J. and Anderson,J.N. (1999) Heterogeneity in the actions of drugs that bind in the DNA minor groove. *Biochemistry*, **38**, 10135–10146.
31. Eriksson,S., Kim,S.K., Kubista,M. and Norden,B. (1993) Binding of 4′,6-diamidino-2-phenylindole (DAPI) to AT regions of DNA: evidence for an allosteric conformational change. *Biochemistry*, **32**, 2987–2998.
32. Zaitsev,E.N. and Kowalczykowski,S.C. (1998) Binding of double-stranded DNA by Escherichia coli RecA protein monitored by a fluorescent dye displacement assay. *Nucleic Acids Res.*, **26**, 650–654.
33. Eggleston,A.K., Rahim,N.A. and Kowalczykowski,S.C. (1996) A helicase assay based on the displacement of fluorescent, nucleic acid-binding ligands. *Nucleic Acids Res.*, **24**, 1179–1186.
34. Bandaru,V., Blaisdell,J.O. and Wallace,S.S. (2006) Oxidative DNA glycosylases: recipes from cloning to characterization. *Methods Enzymol.*, **408**, 15–33.
35. Spackova,N., Cheatham,T.E.III, Ryjacek,F., Lankas,F., Van Meervelt,L., Hobza,P. and Sponer,J. (2003) Molecular dynamics simulations and thermodynamics analysis of DNA-drug complexes. Minor groove binding between 4′,6-diamidino-2-phenylindole and DNA duplexes in solution. *J. Am. Chem. Soc.*, **125**, 1759–1769.
36. Fromme,J.C. and Verdine,G.L. (2003) Structure of a trapped endonuclease III-DNA covalent intermediate. *EMBO J.*, **22**, 3461–3471.
37. Gilboa,R., Zharkov,D.O., Golan,G., Fernandes,A.S., Gerchman,S.E., Matz,E., Kycia,J.H., Grollman,A.P. and Shoham,G. (2002) Structure of formamidopyrimidine-DNA glycosylase covalently complexed to DNA. *J. Biol. Chem.*, **277**, 19811–19816.
38. Holub,O. and Clegg,R.M. (1999), *The 43rd Annual Meeting of the Biophysical Society*. Biophysical Journal (Annual Meeting Abstracts), Baltimore, Maryland, Vol. 76, pp. A129.
39. Porello,S.L., Leyes,A.E. and David,S.S. (1998) Single-turnover and pre-steady-state kinetics of the reaction of the adenine glycosylase MutY with mismatch-containing DNA substrates. *Biochemistry*, **37**, 14756–14764.
40. Williams,S.D. and David,S.S. (1998) Evidence that MutY is a monofunctional glycosylase capable of forming a covalent Schiff base intermediate with substrate DNA. *Nucleic Acids Res.*, **26**, 5123–5133.
41. Williams,S.D. and David,S.S. (1999) Formation of a Schiff base intermediate is not required for the adenine glycosylase activity of Escherichia coli MutY. *Biochemistry*, **38**, 15417–15424.
42. Hashimoto,M., Greenberg,M.M., Kow,Y.W., Hwang,J.T. and Cunningham,R.P. (2001) The 2-deoxyribonolactone lesion produced in DNA by neocarzinostatin and other damaging agents forms cross-links with the base-excision repair enzyme endonuclease III. *J. Am. Chem. Soc.*, **123**, 3161–3162.
43. DeMott,M.S., Beyret,E., Wong,D., Bales,B.C., Hwang,J.T., Greenberg,M.M. and Demple,B. (2002) Covalent trapping of human DNA polymerase beta by the oxidative DNA lesion 2-deoxyribonolactone. *J. Biol. Chem.*, **277**, 7637–7640.
44. Nakano,T., Terato,H., Asagoshi,K., Masaoka,A., Mukuta,M., Ohyama,Y., Suzuki,T., Makino,K. and Ide,H. (2003) DNA-protein

cross-link formation mediated by oxanine. A novel genotoxic mechanism of nitric oxide-induced DNA damage. *J. Biol. Chem.*, **278**, 25264–25272.
45. Ide,H. and Kotera,M. (2004) Human DNA glycosylases involved in the repair of oxidatively damaged DNA. *Biol. Pharm. Bull.*, **27**, 480–485.
46. Travers,A.A. (1989) DNA conformation and protein binding. *Annu. Rev. Biochem.*, **58**, 427–452.
47. Neidle,S. (1992) Minor-groove width and accessibility in B-DNA drug and protein complexes. *FEBS Lett.*, **298**, 97–99.
48. Chuprina,V.P., Heinemann,U., Nurislamov,A.A., Zielenkiewicz,P., Dickerson,R.E. and Saenger,W. (1991) Molecular dynamics simulation of the hydration shell of a B-DNA decamer reveals two main types of minor-groove hydration depending on groove width. *Proc. Natl. Acad. Sci. U.S.A.*, **88**, 593–597.
49. Ghosh,A. and Bansal,M. (1999) C-H.O hydrogen bonds in minor groove of A-tracts in DNA double helices. *J. Mol. Biol.*, **294**, 1149–1158.
50. Van Hecke,K., Nam,P.C., Nguyen,M.T. and Van Meervelt,L. (2005) Netropsin interactions in the minor groove of d(GGCCAATTGG) studied by a combination of resolution enhancement and ab initio calculations. *FEBS J.*, **272**, 3531–3541.